

New All-Atom Force Field for Molecular Dynamics Simulation of an $\text{AlPO}_4\text{-34}$ Molecular Sieve

MATEJ PRAPROTNIK, STANKO HOČEVAR, MILAN HODOŠČEK, MATEJ PENCA, DUŠANKA JANEŽIČ

National Institute of Chemistry, Hajdrihova 19, SI-1000 Ljubljana, Slovenia

Received 3 January 2007; Revised 10 April 2007; Accepted 15 April 2007

DOI 10.1002/jcc.20774

Published online 1 June 2007 in Wiley InterScience (www.interscience.wiley.com).

Abstract: A force field of the triclinic framework of $\text{AlPO}_4\text{-34}$, important in methanol–hydrocarbon conversion reactions, was developed using an empirical potential function. Molecular dynamics simulation of an $\text{AlPO}_4\text{-34}$ triclinic framework segment of 1216 atoms, containing the template molecules isopropylamine and water, was performed with explicit consideration of atomic charges. The average RMS difference between instantaneous positions of the framework atoms during 1 ns simulation and their positions in the structure determined from single crystal X-ray diffraction was calculated, and the average structure of the flexible framework was determined. The computed Debye-Waller factors and simulated FTIR spectra are in good agreement with the experimental data. The new force field permits detailed molecular dynamics simulations of flexible, charged aluminophosphate molecular sieves which should lead to a better understanding of the catalytic processes and the crucial role played by templating molecules.

© 2007 Wiley Periodicals, Inc. J Comput Chem 29: 122–129, 2008

Key words: all-atom force field; molecular dynamics simulation; $\text{AlPO}_4\text{-34}$ molecular sieve

Introduction

Methanol-to-olefin chemistry has attracted substantial interest over the last 15 years not only because of its potential technological and economic value as an alternative route for production of hydrocarbon fuels and basic organic chemicals, but also from the perspective of fundamental research as a means of regulating selectivity in a reaction which proceeds by an unknown mechanism.¹ In the last decade, research in this field has focused around the SAPO-34 silico-alumino-phosphate molecular sieve and its modifications as the most promising catalyst for this process.² It has been known for many years that molecular-shape selective, acid-catalyzed synthesis of ethene and propene from methanol proceeds over some types of zeolite molecular sieves in the hydrogen form, with structures containing relatively small pores. These materials include erionite, zeolite T, chabazite, and ZK-5.³ Unfortunately, the coking of these catalysts is very rapid. The reactions that result in coking are complex and depend on the distribution of strength and concentration of acid sites in a given molecular sieve topology, as well as of the topology itself. The topology determines the possible forms of molecular-shape selectivity constraints imposed on the reactants, products, transition states, and molecular traffic. A judicious combination of all these factors can produce an active, selective, and stable catalyst for methanol-to-olefin conversion.⁴

Aluminophosphates contain a series of 8-membered rings composed of 8-tetrahedrally coordinated alternating aluminum and phosphorus atoms.

The diameter of this 8-membered ring, i.e., the distance between the centers of oxygen atoms in the ring minus twice the radius of the oxygen ion is crucial to the catalytic performance of molecular sieves. Single-crystal X-ray diffraction data for SAPO-34 and CoAPSO-34 have shown that in chabazite-like materials such as SAPO-34 or MeAPSO-34 (Me=Co, Mn, Cr, Ni) and SAPO-44 or MeAPSO-44 (Me=Co, Mn) the root-mean-square diameter of the 8-membered ring (Fig. 3a) is 0.4300 and 0.4304 nm, respectively. The kinetic diameters of species found in the gas phase of the reaction system are 0.363 nm for methanol, 0.431 nm for dimethyl ether, 0.264 nm for water, 0.416 nm for ethene, 0.444 nm for ethane, and 0.468 nm for propene; and the higher propensity of these molecular sieves for ethene formation appears to be the consequence of the close match between the 8-membered ring aperture and the kinetic diameter of the reactant and product molecules.⁵ After studying the differ-

Correspondence to: D. Janežič; e-mail: dusa@cmm.ki.si

Contract/grant sponsor: Slovenian Research Agency; contract/grant numbers: P1-0002, P2-0152

ence between the activity and selectivity towards ethene formation in the same reaction over the two series of the first row transition-metal substituted silicoaluminophosphate molecular sieve, namely MeAPSO-34 (Me=Co, Mn, Cr), SAPO-34, and MeAPSO-44 (Me=Co, Mn, Cr, Zn, Mg), SAPO-44, it was concluded that there is no difference in activity between the comparable transition-metal substituted samples. It was found however⁶ that there is an almost threefold difference in selectivity to ethene between the MeAPSO-44 and the MeAPSO-34 structures and this was ascribed to the 0.009 nm difference in the 8-membered ring apertures. It was also found that the selectivity of this catalyst for ethene follows the Irving-Williams order of ligand field stabilization energies (LFES), characteristic for coordination compounds. The transition metals incorporated into the aluminophosphate or silicoaluminophosphate frameworks behave as coordinately unsaturated species with an aluminophosphate framework present as a quadridentate ligand.⁶

A major step forward in understanding the origins of product selectivity in methanol-to-olefin chemistry with the HSAPO-34 molecular sieve catalyst has been made recently using GC volatile products analysis in tandem with ^{13}C solid-state MAS NMR analysis of the quenched reaction products within the molecular sieve nanocages.^{7,8} These experiments revealed that under the given experimental conditions, the catalytically active sites are self-assembled within the chabazite-like nanocages of HSAPO-34. Here, they first form methylbenzenes that are trapped like a ship-in-a-bottle within the nanocages where they are easily converted to carbenium ions through interaction with methoxonium or hydroxonium ions. It was also demonstrated that methylbenzenes having two- or three-methyl groups are converted preferentially to ethene, while methylbenzenes having four- to six-methyl groups produce propene. This behavior of the HSAPO-34 active site can be seen as elegant as that of an enzyme.

In an effort to understand structure and catalysis on transition metal substituted aluminophosphate molecular sieves, we decided to use molecular dynamics (MD) simulation. This would allow decoupling of the effect of isomorphously substituted transition elements with the associated acidity function and unsaturated coordination from the molecular-shape selectivity function, the effect of framework topology. The MD simulation of zeolite and aluminophosphate molecular sieve frameworks is a prerequisite of any serious attempt to interpret or predict the diffusion, adsorption, and reaction of organic and inorganic molecules within these spatially constrained systems. Recent simulations of such reaction systems under conditions in which the molecular sieve framework is allowed to relax, have shown that the dynamics of the guest molecule are substantially altered.⁹ This is expected when the size of the guest molecule approaches the size of the framework channel or window, since the view of the molecular sieve lattice as rigid ignores not only the motion of the framework atoms but also energy exchange between guest and host and the dynamic coupling of the vibrations of the adsorbate and the framework.¹⁰ Such simulations with the framework flexibility included, however, are computationally very demanding as a result of the large number of degrees of freedom that must be considered. Until recently, such calculations have been prohibitively expensive and available only to the research

groups with access to large computing facilities. Parallel computing based on point to point parallel architectures of PC clusters removes this problem and allows performance of tasks that are very CPU-intensive [CROW-4 (Column and Rows of Workstations) is a 6 dimensional hypercube cluster of PC processors].¹¹ A different problem hindering MD simulation is the lack of an effective force field, which describes the interactions between the atoms of the system. The density functional theory (DFT)^{12–16} and other *ab initio*^{17–19} approaches of course provide the most accurate description of interactions because they are calculations based on first principles and require no experimental data to determine the interatomic forces. However, they are often computationally too expensive for the modeling of zeolite and aluminophosphate molecular sieve frameworks. The classical force field calculations are much cheaper and allow us to study larger systems. The CHARMM energy function²⁰ and the more recent Universal force field²¹ approaches have been used extensively in the molecular mechanics and MD simulations of organic and inorganic macromolecular systems. Many force field MD simulations have been performed on zeolites and aluminophosphates, see for example refs. 22–28.

The objective of the present study was a development of a new all-atom force field for MD simulation of the as-synthesized $\text{AlPO}_4\text{-34}$ triclinic molecular sieve including isopropylamine template and associated water molecules. Our force field includes a full framework flexibility modeled via harmonic bond stretching and angle bending potential terms as well as electrostatic and van der Waals interactions between the aluminophosphate molecular sieve and the isopropylamine template and associated water molecules. Using the newly developed force field an MD simulation of this system was performed, using a segment of 1216 atoms representing one chabazite-type cavity surrounded by one layer of equal chabazite-type cavities, which is an adequate representation of the crystal environment. The results of these calculations were compared with the X-ray single crystal data. In addition, the Fourier transform of the charge-weighted velocity autocorrelation function was compared with the Fourier transform infrared (FTIR) spectrum of the as-synthesized $\text{AlPO}_4\text{-34}$ molecular sieve. MD studies of methanol dehydration on a silicon- and transition metal-substituted framework will be completed in a separate study.

Experimental Section

Crystallographic Data

A $0.126 \times 0.078 \times 0.155 \text{ mm}^3$ crystal of as-synthesized triclinic $\text{AlPO}_4\text{-34}$ (Fig. 1) was used to collect intensity data with MoK_α radiation ($\lambda = 0.071069 \text{ nm}$) on an Enraf-Nonius CAD4 diffractometer.

The triclinic unit cell, obtained on the basis of 75 reflections in the 2θ range of $16.446^\circ\text{--}29.800^\circ$, using the least squares method has the following parameters: $a = 0.9117(1) \text{ nm}$, $b = 0.9240(1) \text{ nm}$, $c = 0.9356(1) \text{ nm}$, $\alpha = 86.74(1)^\circ$, $\beta = 80.04(1)^\circ$, $\gamma = 87.91(1)^\circ$, $V = 0.7748(2) \text{ nm}^3$. The space group is $P\bar{1}$.²⁹ The unit cell is composed of two asymmetric units ($Z = 2$). The

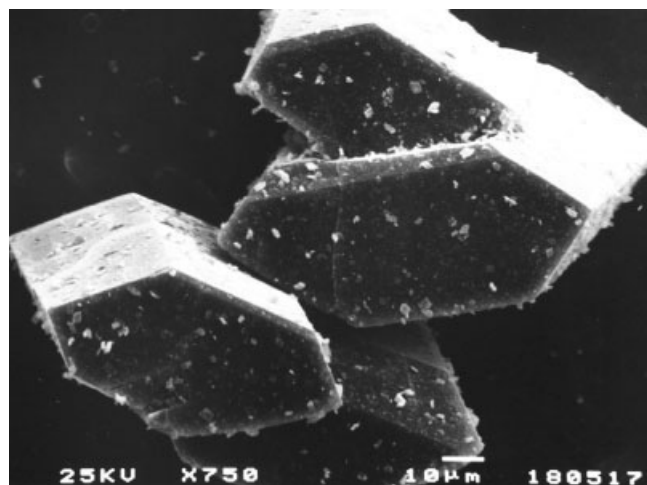


Figure 1. SEM image of as-synthesized triclinic AlPO₄-34 crystals.

framework consists of cross-linked PO₄-tetrahedra, AlO₄-tetrahedra and AlO₄F₂-octahedra to produce three-dimensional interconnecting channel systems, all formed by 8-ring apertures: {⊥[100] 84.1 × 4.7 ↔ ⊥[010] 83.6 × 5.0 ↔ ⊥[001] 82.9 × 4.8} (The crystallographic characterization of the channels is written according to the notation in ref. 30). Two diagonally opposed aluminium atoms in a 4-membered ring are bridged by two fluorine atoms positioned in plane with two bridging oxygen atoms per each aluminium atom. Both aluminium atoms are thus octahedrally coordinated sharing common F—F edge of two, almost ideal, octahedra. The ratio of tetrahedrally to octahedrally coordinated aluminium is 2:1. Two protonated isopropylamine molecules and two water molecules are located in one chabazite-like cage. The protonated amino group in isopropylamine is hydrogen bonded to one bridging fluoride ion protruding into the cage, to the oxygen positioned in plane with fluoride, and to the nearby water molecule. The oxygen atom of the water molecule is disordered between two positions, one 50% and the other 22% occupied. The stoichiometry of H₂O:Pr¹NH₃⁺:F⁻ is 1:1:1.²⁹

FTIR Spectrum

A finely grained powder of as-synthesized AlPO₄-34 containing isopropylamine and water template molecules was mixed with KBr powder and a pellet was formed. The Fourier transform infrared spectra (FTIR) were scanned in the near infrared region (150–700 cm⁻¹) and in middle infrared region (400–4000 cm⁻¹) on a Perkin-Elmer System 2000 spectrometer with resolution of 2 cm⁻¹.

Computational Methods

Force Field Development

To study the effect of the aluminophosphate framework dynamics on the mechanism of methanol dehydration reaction by MD simulation a force field was developed for the AlPO₄-34 triclinic frame-

work. The energy function as implemented in CHARMM²⁰ was used to describe the interactions between all atoms in the system:

$$E = \sum_i \frac{p_i^2}{2m_i} + \sum_{\text{bonds}} k_b(r - r_0)^2 + \sum_{\text{angles}} k_\theta(\theta - \theta_0)^2 + \sum_{i>j} \frac{q_i q_j}{4\pi\epsilon_0 r_{ij}} + \sum_{i>j} 4\epsilon_{ij} \left[\left(\frac{\sigma_{ij}}{r_{ij}} \right)^{12} - \left(\frac{\sigma_{ij}}{r_{ij}} \right)^6 \right] \quad (1)$$

where p_i is the linear momentum of the i th atom, m_i is its mass, r_0 and θ_0 are reference values for bond lengths and angles, respectively, k_b and k_θ are corresponding force constants; i and j run over all atoms, q_i denotes the charge on the i th atom and r_{ij} is the distance between the i th and j th atom, ϵ_{ij} and σ_{ij} are the corresponding constants of Lennard-Jones potential. The first term in eq. (1) represents the kinetic energy of the system, the second, the bond stretching potential, and the third, the bond angle potential. The last two terms are the electrostatic and Lennard-Jones potential, respectively. The dihedral degrees of freedom and the corresponding torsional potential were omitted because of rigidity imposed by the framework structure. Electrostatic interactions are explicitly taken into account for 1–4 neighbors and higher; the electrostatic interactions between 1–2 and 1–3 neighbors are included implicitly in the bond stretching and angle bending terms.

The unknown stretching and bending force constants and the framework atoms' charges were calculated as follows. The asymmetric unit (Fig. 2) was taken as the building block of the AlPO₄-34 triclinic framework.

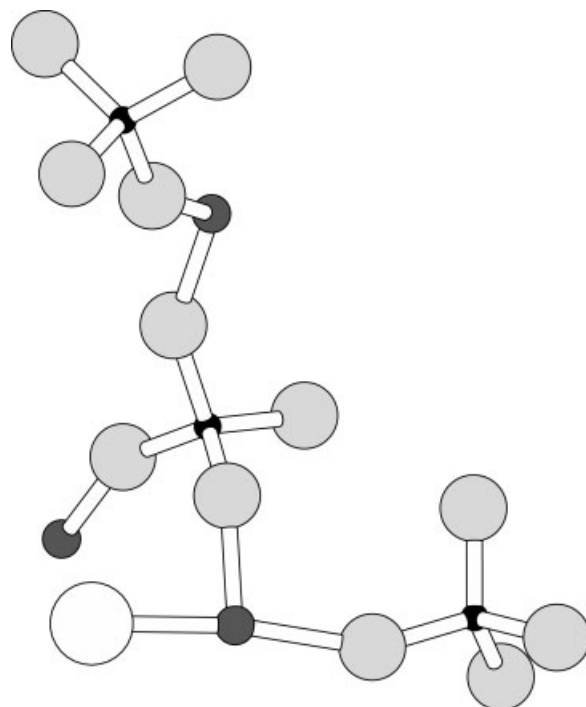


Figure 2. Asymmetric unit: small black balls—P; middle black balls—Al; large grey balls—O; large white ball—F.

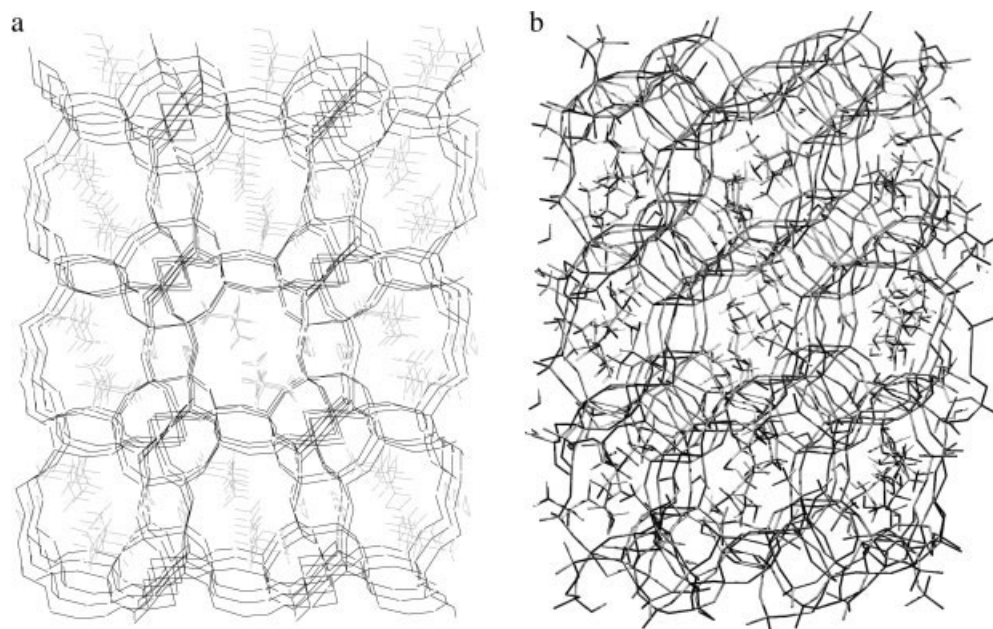


Figure 3. (a) Structure of the as-synthesized triclinic $\text{AlPO}_4\text{-34}$ according to single crystal diffraction data (view along [100] direction). (b) Minimized energy structure of the $\text{AlPO}_4\text{-34}$ obtained after the ABNR minimization on a segment of 1216 framework atoms.

The coordinates of the atoms that constitute this unit were determined from single crystal X-ray data.²⁹ The structure of an as-synthesized triclinic $\text{AlPO}_4\text{-34}$ viewed along the 100 direction is presented in Figure 3a.

Recent force fields of aluminophosphate frameworks in which coulombic interaction is completely neglected³¹ have been developed for neutral template molecules with no large electric dipoles or quadrupoles. However, because of large electric dipoles of water molecules, which in this study were added to the template molecules, the explicit coulombic interactions with the framework atoms must be considered and consequently, the unknown charges of the framework atoms must be determined. This was accomplished using the Mulliken population analysis of a cluster of 54 atoms cut out of the framework. Hydrogen atoms were placed on the free binding sites to complete the cluster and were summed into heavy atoms.

Table 1 presents the charges of the framework atoms. The parameters of the template molecule, isopropylamine, were taken from the CHARMM force field,²⁰ and a TIPS3P potential was used for water molecules.

To make the new force field transferable to the other aluminophosphate frameworks, smaller clusters, e.g., AlO_4 , O-Al-O , F-Al-O , P-O-Al , Al-F-Al , and F-Al-F , which constitute the asymmetric unit of the $\text{AlPO}_4\text{-34}$ triclinic molecular sieve and are also found in other aluminophosphate frameworks, were chosen as model systems for determination of the unknown force constants. The normal mode frequencies³² of these smaller clusters depend on the unknown force constants. The latter were determined by fitting the normal mode frequencies, computed using CHARMM, to the normal mode frequencies computed quantum-mechanically at the B3LYP/6-31G*

level by GAUSSIAN 98.³³ The reference values for bond lengths and angles were determined from single crystal X-ray diffraction data.²⁹ All other parameters were taken from the CHARMM force field.²⁰

MD Simulation Calculations

A segment of 1216 atoms represents one chabazite-type cavity surrounded with one layer of equal chabazite-type cavities, which represents the crystal environment adequately. Two isopropylamine and two water molecules per cavity were embedded into the framework. First, 10,000 steps of the ABNR (adopted basis Newton-Raphson) minimization²⁰ with the framework fixed were performed to rearrange the template molecules correctly into the framework environment. Then an additional 10,000 steps of the ABNR minimization with a flexible framework were performed to give the structure shown in Figure 3b. The average RMS difference between the framework atoms'

Table 1. Charges of Framework Atoms P, Al, O, F in Elementary Charge Units.

Atom	Charge (e_0)
P	+1.85
Al	+1.37
O	-0.76
F	-0.54

Table 2. Force Constants (k_b) and Reference Bond Lengths (l_0) for P–O, Al–O, and Al–F Bonds.

Bond	k_b (kJ mol ⁻¹ nm ⁻²)	l_0 (nm)
Al–O	87,780	0.17700
P–O	160,930	0.15250
Al–F	141,075	0.18937

positions in the resulting minimized energy structure and their positions in the structure determined from single crystal X-ray diffraction was 0.16 nm. This minimized structure was taken as the starting structure for the MD simulation. The equations of motion were integrated using the standard velocity Verlet algorithm with the time step of 1 fs, no periodic boundary conditions and no cut-off or symmetry constraints were imposed; the atoms were allowed to move during the simulation only subject to the interatomic interactions.

The system was first equilibrated for 20 ps from an initial temperature of 100 K to the final temperature of 300 K while atom velocities were scaled every 1000th integration step. Then 100 ps of canonical equilibration followed while atom velocities were again scaled every 1000th integration step to ensure that the atom velocities at the end of the simulation, at a temperature of 300 K, assume a Maxwell distribution. Finally, a microcanonical NVE ensemble production run of 50 ps at $T = 300$ K was performed with an initial set of force constants obtained from quantum-mechanical calculation, as previously described. Then the FTIR spectrum as a Fourier transform of the charge-weighted velocity autocorrelation function^{31,34} was computed and the resulting spectrum compared to the experimental spectrum. The force constants were then adjusted in an iterative way, i.e., repeating the simulation steps described above using the corrected force constants as an input at each iteration until the IR band positions of both the calculated and experimental spectrum overlapped.³⁵ The values of the force constants determined in this way, the atomic charges, which were computed quantum-mechanically, and the reference values for bond lengths and angles used in eq. (1) are given in Tables 2 and 3.

Further MD calculations were performed with these force constants using the same procedure: 20 ps of equilibration from the initial temperature of 100 K to a final temperature of 300 K, 100 ps of canonical equilibration run at $T = 300$ K, and the NVE production run of 1 ns at $T = 300$ K. All MD calculations were performed using CHARMM program version c27a1.

There being no periodical boundary conditions imposed in the simulation, we tested the reliability of our approach by performing the MD simulation with the production run of 100 ps on a larger segment of 6318 atoms representing one chabazite-type cavity surrounded with two layers of equal chabazite-type cavities ($5 \times 5 \times 5$ chabazite cavities). The convergence of results in both cases ($3 \times 3 \times 3$ and $5 \times 5 \times 5$ segments) was satisfactory, indicating that environment of the central chabazite-type cavity is essentially the same in both cases. This similarity indicates that a sufficiently large segment as a model is a satisfactory surrogate for a periodical boundary condition.

Results and Discussion

The SEM view of the monocrystals of the as-synthesized AlPO₄-34 triclinic molecular sieve is shown in Figure 1. A monocrystal with dimensions of approximately 0.15 mm was used for the collection of single crystal diffraction data. The framework structure and the positions within of isopropylamine and water template molecules, obtained from diffraction data, are presented in Figure 3a as the view along [100] axis. The minimum energy structure for a segment of 1216 framework atoms together with both template molecules embedded into the framework (2 isopropylamine and 2 water molecules per chabazite-type cavity), calculated using the ABNR minimization is shown in Figure 3b.

The RMS difference between the instantaneous framework atoms' position in the simulation run and their positions in the structure as determined by single crystal X-ray diffraction were computed, and the average structure of the central asymmetric unit during the production run of 1 ns at 300 K was determined (Table 4).

After a 400 ps production run, the framework with template molecules reaches equilibrium with an RMS of about 0.18 nm as shown in Figure 4. Nevertheless, the RMS difference computed for the atoms from the central cavity is as expected smaller (0.05 nm) due to the movement of the outer atoms in the framework.

The same RMS difference was also computed for the framework in the absence of template molecules. Without template molecules, the framework shows an increase in RMS, which begins after the production run of about 220 ps (Fig. 4). This demonstrates that our model correctly predicts the experimental fact that the template molecules stabilize the framework at this temperature. The Debye-Waller factors computed from the mean-square atomic fluctuations for the atoms of the central asymmetric unit in this production run are given in column 3 of Table 5 and are compared to the Debye-Waller factors obtained from single crystal XRD data (column 2). A good agreement between the simulation and experimental data is found. This indicates that our newly developed force field is accurate enough to calculate small differences pore openings.

The IR spectrum is a fingerprint of a compound or a complex system. The computation of the IR spectra from the MD data using a Fourier transform of the charge-weighted velocity autocorrelation function has been established as one method of verifying the correctness of the performed MD calculations.^{36–38}

Table 3. Force Constants (k_θ) and Reference Bond Angles (θ_0) for O–Al–O, P–O–Al, O–P–O, O–Al–F, Al–F–Al, and F–Al–F Angles.

Angle	k_θ (kJ mol ⁻¹ deg ⁻¹)	θ_0 (deg)
O–Al–O	73.15	106.5
P–O–Al	148.39	146.6
O–P–O	271.70	109.9
O–Al–F	129.58	90.9
Al–F–Al	83.60	100.7
F–Al–F	156.75	79.2

Table 4. Atomic Positional Parameters (Fractional Coordinates) of the Central Asymmetric Unit as Obtained from Single Crystal XRD Data (Experimental) and as Calculated from the Average Atomic Positions After 1 ns Production Run at $T = 300$ K (Calculated).

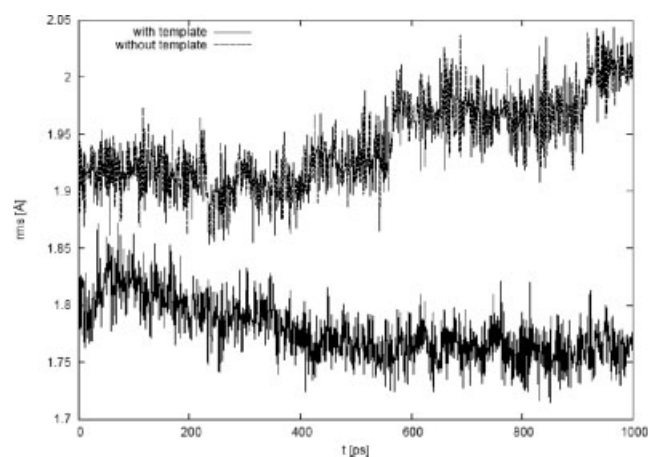
Atom	x/a		y/b		z/c	
	Experimental	Calculated	Experimental	Calculated	Experimental	Calculated
P(1)	0.36842	0.37317	0.61826	0.65074	0.68137	0.67967
P(2)	0.16672	0.16315	0.65633	0.66500	0.13728	0.10241
P(3)	0.38408	0.38354	0.18599	0.16040	0.88962	0.91198
Al(1)	0.40109	0.40769	0.63360	0.64872	0.34293	0.32437
Al(2)	0.35674	0.39056	0.84722	0.87422	0.92393	0.93381
Al(3)	0.13381	0.15634	0.44265	0.44524	0.90995	0.92199
O(1)	0.24403	0.23269	0.51707	0.57851	0.74137	0.77319
O(2)	0.36587	0.39830	0.75365	0.78981	0.76745	0.75833
O(3)	0.35628	0.35603	0.66910	0.68936	0.52532	0.51843
O(4)	0.52136	0.51170	0.54126	0.54683	0.68028	0.67883
O(5)	-0.00087	-0.00731	0.64749	0.67029	0.18601	0.14006
O(6)	0.23397	0.19778	0.53845	0.53463	0.03575	0.00680
O(7)	0.20679	0.22738	0.80586	0.80389	0.06033	0.01359
O(8)	0.23645	0.23835	0.64289	0.65172	0.27598	0.24221
O(9)	0.24411	0.24357	0.27604	0.26387	0.92991	0.95131
O(10)	0.34463	0.33688	0.02933	0.00341	0.87405	0.89282
O(11)	0.47629	0.48520	0.23860	0.22177	0.74500	0.77199
O(12)	0.47719	0.47508	0.19085	0.15136	1.01159	1.03768
F	0.00159	-0.05154	0.60602	0.49090	0.91804	0.97668

The experimental FTIR spectrum of the as-synthesized triclinic $\text{AlPO}_4\text{-34}$ molecular sieve is given in Figure 5a and its computed counterpart at 300 K in Figure 5b. The main features of the experimental FTIR spectrum are reproduced well in the computed spectrum. The bands in the experimental FTIR spectrum are consistently broader than the computed bands because the experimental spectra shows broadening resulting from the inhomogeneity of crystals, an imperfection absent in the model, which assumes a perfect crystal. Nevertheless, the bands in the

experimental spectrum at 1098, 1067, 1035, and 989 cm^{-1} correspond to bands in the computed spectrum of the asymmetric unit and of the framework at 1093, 1073, 1040, and 1000 cm^{-1} attributable to the asymmetric and symmetric stretch vibrations of the PO_4 and AlO_4 tetrahedra.

Table 5. Isotropic Displacement (\AA^2) (Debye-Waller Factors) for the Atoms of the Central Asymmetric Unit as Obtained from Single Crystal XRD Data (Experimental) and as Calculated from the Average Atomic Positions After 1 ns Production Run at $T = 300$ K (Calculated).

Atoms	$U_{\text{experimental}}$	$U_{\text{calculated}}$
P(1)	0.00694(8)	0.00818
P(2)	0.00740(9)	0.00920
P(3)	0.00727(8)	0.00874
Al(1)	0.00792(10)	0.00823
Al(2)	0.00725(10)	0.00893
Al(3)	0.00749(10)	0.00749
O(1)	0.01309(25)	0.01001
O(2)	0.01432(25)	0.01110
O(3)	0.01483(25)	0.01038
O(4)	0.01564(25)	0.01094
O(5)	0.01045(24)	0.01165
O(6)	0.01146(24)	0.01126
O(7)	0.01418(25)	0.01226
O(8)	0.0164(3)	0.01259
O(9)	0.01342(25)	0.01074
O(10)	0.01611(25)	0.01191
O(11)	0.01644(25)	0.01166
O(12)	0.0189(3)	0.01247
F	0.01020(20)	0.01561

**Figure 4.** RMS (\AA) of atomic positions in the framework with templates and in the framework without templates obtained from MD calculations with respect to the atomic positions obtained from single crystal XRD data.

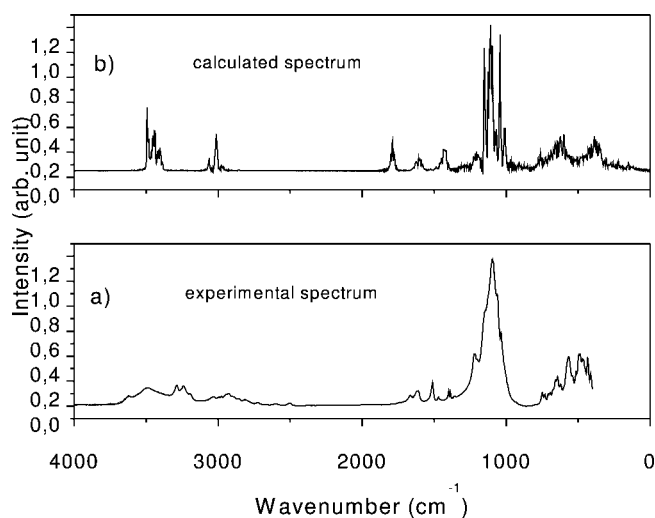


Figure 5. Experimental (a) and calculated (b) spectra of as-synthesized triclinic $\text{AlPO}_4\text{-34}$ molecular sieve.

The assignment of bands below 1000 cm^{-1} to the specific framework vibrational modes is uncertain because of their superposition on the vibrational modes of both templates—water and isopropylamine.

From the point of view of molecular sieve topology, a structure can be represented as a superposition of prenucleation building units into frameworks of limited number of space group,³⁹ as has been experimentally confirmed by *in situ* high resolution multinuclear NMR of hydrothermal crystallogensis. One might then expect to observe a localized vibration of a specific structural unit that would be a linear combination of a small number of normal modes of the lattice, similar to the group frequency approach widely employed in the interpretation of the vibrational spectra of organic molecules. The IR spectrum could then be used to identify the molecular sieve topology and its origin, the integrand unit.

To assign a specific band to the particular linear combination of normal modes of the lattice, we also compared the computed spectrum of the 1216 atom framework with that of the asymmetric unit that was used to generate this framework. From these spectra, which are presented in Figures 6a and 6b, it can be seen that there are some differences in both position and intensity of the bands. The bands at 1147 , 1123 , 1108 , and 765 cm^{-1} in the computed spectrum of the framework are absent from the computed spectrum of the asymmetric unit. Also, the bands at 797 and 312 cm^{-1} in the computed spectrum of the asymmetric unit, are absent from the spectrum of the framework.

Evidently, the spectrum of the framework gives different bands and these can be the consequence of different linear combinations of the same “elementary” normal modes found in the asymmetric unit or the outcome of linear combinations of different normal modes in these two entities. Therefore, whether or not specific bands in the spectrum of the framework can be ascribed to the specific secondary building units remains an open question.

Conclusions

An as-synthesized $\text{AlPO}_4\text{-34}$ triclinic molecular sieve including template isopropylamine and water molecules has been studied by MD simulation. An empirical CHARMM-like force field including a bond stretching, angle bending, Lennard-Jones and also a Coulomb potential term for this fully flexible framework was developed for this purpose. The unknown force constants and the charges on the framework atoms were determined using experimental data and *ab-initio* quantum chemical calculations. Determination of the charges on the atoms of the flexible framework was necessary because of the electrostatic interactions between the framework and the polar water molecules. With this newly developed force field, a 1 ns long MD simulation was successfully performed on a segment of 1216 atoms, representing one chabazite-type cavity surrounded by one layer of equal chabazite-type cavities, with two template isopropylamine and two water molecules per cavity at the temperature 300 K. This force field appears to be applicable to any aluminophosphate framework.

From a comparison of the MD-computed and the X-ray positions of the framework atoms, it is evident that the templating molecules stabilize the framework. The results also indicate that the computed Debye-Waller factors and the IR spectra are in good agreement with the experimental data. This proves that the structure and dynamics of the as-synthesized $\text{AlPO}_4\text{-34}$ triclinic molecular sieve are described satisfactorily by the new empirical potential function.

The computed IR spectra also provide an opportunity to interpret the experimental IR spectra. Comparison of the computed spectrum of the framework with that of the asymmetric unit that was used to generate this framework allowed assignment of specific bands in the IR spectrum to a particular linear combination of normal modes of the framework. Differences between these two spectra were seen and whether or not the specific bands in the spectrum of framework can be ascribed to the

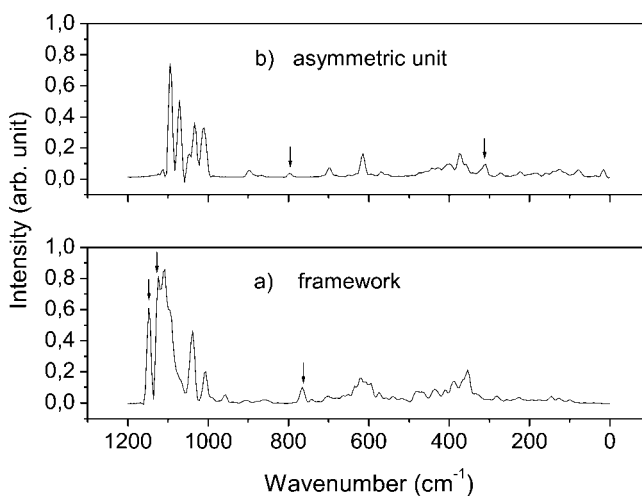


Figure 6. Calculated spectra of the framework (a) and of the asymmetric unit (b) from the same MD production run. Arrows depict the bands that differ in the two spectra and are described in the text.

specific secondary building units can not be answered definitively in the absence of further data. With the new force field in hand however, further MD simulations (also with the periodic boundary conditions implementation), which become quite straightforward, will lay the groundwork that will lead to answers to these questions.

References

1. Stöcker, M. *Microporous Mesoporous Mater* 1999, 29, 3.
2. Hartmann, M.; Kevan, L. *Chem Rev* 1999, 99, 635.
3. Chang, C. D. *Hydrocarbons from Methanol*, Chemical Industries, Vol. 10; Marcel Dekker: New York, 1983.
4. Hočevar, S.; Batista, J. In *Advances in Catalyst Design*; Graziani, M.; Rao, C. N. R., Eds.; World Scientific: Singapore, 1991; pp. 137–146.
5. Hočevar, S.; Levec, J. *J Catal* 1992, 135, 518.
6. Hočevar, S.; Batista, J.; Kaučič, V. *J Catal* 1993, 139, 351.
7. Song, W.; Haw, J. F.; Nicholas, J. B.; Heneghan, C. S. *J Am Chem Soc* 2000, 122, 10726.
8. Song, W.; Fu, H.; Haw, J. F. *J Am Chem Soc* 2001, 123, 4749.
9. Štich, I.; Gale, J. D.; Terakura, K.; Payne, M. C. *J Am Chem Soc* 1999, 121, 3292.
10. Bates, S. P.; Van Santen, R. A. *Adv Catal* 1998, 42, 1.
11. Borštnik, U.; Hodošček, M.; Janežič, D. *J Chem Inform Comput Sci* 2004, 44, 359.
12. Catlow, C. R. A.; French, S. A.; Sokol, A. A.; Thomas, J. M. *Philos Trans R Soc London A* 2005, 363, 913.
13. Hafner, J.; Bencko, L.; Bučko, T. *Top Catal* 2006, 37, 41.
14. Poulet, G.; Sautet, P.; Tuel, A. *J Phys Chem* 2002, 106, 8599.
15. Blaszkowski, S. R.; van Santen, R. A. *J Phys Chem* 1995, 99, 11728.
16. Car, R.; Parrinello, M. *Phys Rev Lett* 1985, 55, 2471.
17. Termath, V.; Haase, F.; Sauer, J.; Hutter, J.; Parrinello, M. *J Am Chem Soc* 1998, 120, 8512.
18. Cora, F.; Catlow, C. R. A. *J Phys Chem B* 2003, 107, 11861.
19. Cora, F.; Catlow, C. R. A.; Civalieri, B.; Orlando, R. *J Phys Chem B* 2003, 107, 11866.
20. Brooks, B. R.; Bruccoleri, R. E.; Olafson, B. D.; States, D. J.; Swaminathan, S.; Karplus, M. *J Comput Chem* 1983, 4, 187.
21. Rappé, A. K.; Casewit, C. J.; Colwell, K. S.; Goddard, W. A., III; Skiff, W.; Uff, M. *J Am Chem Soc* 1992, 114, 10024.
22. Liu, B.; Smit, B.; Calero, S. *J Phys Chem B* 2006, 110, 20166.
23. Dubbeldam, D.; Calero, S.; Vlugt, T. J. H.; Krishna, R.; Maesen, T. L. M.; Beerdsen, E.; Smit, B. *Phys Rev Lett* 2004, 93, 088302–1.
24. Ermoshin, V. A.; Smirnov, K. S.; Bougeard, D. *Chem Phys* 1996, 209, 41.
25. Ermoshin, V. A.; Smirnov, K. S.; Bougeard, D. *Chem Phys* 1996, 202, 53.
26. Gale, J. D.; Henson, N. J. *J Chem Soc Faraday Trans* 1994, 90, 3175.
27. Gale, J. D. *J Chem Soc Faraday Trans* 1997, 93, 629.
28. Gale, J. D.; Rohl, A. L. *Mol Simulat* 2003, 29, 291.
29. (a) Hočevar, S.; Batista, J. *Pat. SI* 9,300,447 A, August 25, 1993; (b) Logar, N. Z. *Structural Characterisation of Phosphate-Based Molecular Sieves*, PhD Thesis, University of Ljubljana, Faculty of Chemistry and Chemical Technology, Ljubljana, 1998.
30. Meier, W. M.; Olson, D. H. *Atlas of Zeolite Structure Types*, 3rd ed., Butterworth-Heinemann: London, 1992. *Zeolites*, 12(5), Special Issue.
31. Demontis, P.; Gulin Gonzales, J.; Suffriti, G. B.; Tilloca, A.; de las Pozas, A. *Microporous Mesoporous Mater* 2001, 42, 103.
32. Brooks, B. R.; Janežič, D.; Karplus, M. *J Comput Chem* 1995, 16, 1522.
32. Frisch, M. J.; Trucks, G. W.; Schlegel, H. B.; Scuseria, G. E.; Robb, M. A.; Cheeseman, J. R.; Montgomery, J. A.; Vreven, T.; Kudin, K. N.; Burant, J. C.; Millam, J. M.; Iyengar, S. S.; Tomasi, J.; Barone, V.; Mennucci, B.; Cossi, M.; Scalmani, G.; Rega, N.; Petersson, G. A.; Nakatsuji, H.; Hada, M.; Ehara, M.; Toyota, K.; Fukuda, R.; Hasegawa, J.; Ishida, M.; Nakajima, T.; Hona, Y.; Kitao, K.; Nakai, H.; Klene, M.; Li, X.; Knox, J. E.; Hratchian, H. P.; Cross, J. B.; Adamo, C.; Jaramillo, J.; Gomperts, R.; Stratmann, R. E.; Yazyev, O.; Austin, A. J.; Cammi, R.; Pomelli, C.; Ochterski, J. W.; Ayala, P. Y.; Morokuma, K.; Voth, G. A.; Salvador, P.; Dannenberg, J. J.; Zakrzewski, V. G.; Dapprich, S.; Daniels, A. D.; Strain, M. C.; Farkas, O.; Malick, D. K.; Rabuck, A. D.; Raghavachari, K.; Foresman, J.; Ortiz, J. V.; Cui, Q.; Baboul, A. G.; Clifford, S.; Cioslowski, J.; Stefanov, B. B.; Liu, G.; Liashenko, A.; Piskorz, P.; Komaromi, I.; Martin, R. L.; Fox, D. J.; Keith, T.; Al-Laham, M. A.; Peng, C. Y.; Nanayakkara, A.; Challacombe, M.; Gill, P. M. W.; Johnson, B.; Chen, W.; Wong, M. W.; Gonzalez, C.; Pople, J. A. *Gaussian 03 (revision B.04)*, Gaussian, Inc.: Pittsburgh, PA, 2003.
34. Bornhauser, P.; Bougeard, D. *J Phys Chem B* 2001, 105, 36.
35. Praprotnik, M.; Janežič, D.; Mavri, J. *J Phys Chem A* 2004, 108, 11056.
36. Janežič, D.; Praprotnik, M.; Merzel, F. *J Chem Phys* 2005, 122, Article Number 174101.
37. Praprotnik, M.; Janežič, D. *J Chem Phys* 2005, 122, Article Number 174102.
38. Praprotnik, M.; Janežič, D. *J Chem Phys* 2005, 122, Article Number 174103.
39. Vistad, O. B.; Akporiaye, D. E.; Taulelle F.; Lillerud, K. P. *Chem Mater* 2003, 15, 1639.